Prior Models On Coronary Arteries
CS 446 Computer Integrated Surgery II
Project Final Report, 09 May 2012

Mehmet Akif Gulsun

Mentor: Gareth Funka-Lea, Siemens Corporation, Corporate Research, Princeton

Abstract

Detection of coronary arteries from medical image data and their statistical analysis are difficult tasks due to the large variation in their anatomy. The goal of this project is to investigate models for characterizing coronary arteries that can be used as prior models to support their detection in computed tomography angiography (CTA) scans and to allow for their statistical analysis. In the first part of this project, I look into statistics on territories by computing coronary average density map in a canonical coordinate system. In the second part, I build tree-shape models and compute geodesic deformation between them with two different metrics that can account for the variation in the tree-shape topology. Finally, I apply these tree-shape geodesic metrics for coronary tree matching and average tree computation. The methods are tested on 50 hand annotated coronary centerlines giving very promising results.

1 Introduction

1.1 Motivation

According to American Heart Association, coronary artery disease (CAD) is a leading cause of death among cardiovascular diseases in the United States [1]. This fact puts emphasize on the necessity of its diagnosis, treatment and monitoring for which computed tomography angiography (CTA) is considered as the primary imaging modality because of its superior image resolution. In addition, recent advancements in CTA technology allows scans with significantly reduced radiation which encourages routine screenings. However, due to thin and longitudinal anatomy of coronary arteries, CTA data itself is difficult and time-consuming to be interpreted by the operators without additional post-processing. Therefore, detection of coronaries in CTA is needed for advanced visualization and quantification purposes. Figure 1a shows an example of three-dimensional CTA volume with coronary artery centerlines overlaid.

Detected coronary centerlines can facilitate the diagnosis and treatment process by several means. First, they are used in advanced visualization in order to provide a quick overview of coronaries to the physicians, Figure 1b. Second, centerlines are used in extracting 3D model geometry of the coronary artery where this model is used for different purposes such as stenonis quantification or stent planning, Figure 1c. Finally, the centerlines are also used for intra-operative catheter guidance by registering and overlaying them onto live X-ray images.
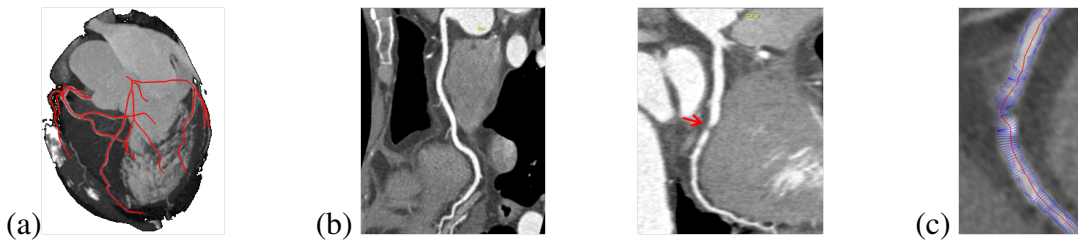
Figure 1: a) Sample CTA volume visualized within cropped heart mask using maximum intensity projection (MIP). Coronary centerlines are overlaid in red. b) Curved multi-planar reformat images that are reconstructed from the right coronary centerlines. The red arrow in the second image depicts a stenosis in the coronary branch. c) 2D cross-sectional vessel contours along the coronary centerline with stenosis.

In spite of the good image quality in CTA data, irregular topology of coronary anatomy, pathologies and imaging artifacts make coronary detection a challenge. Coronary prior models that are capable of capturing anatomical variations in the population can improve the detection by guiding commonly used local tracking methods or by supporting the prediction of global classification methods. Besides detection, statistical analysis of coronaries is also a challenge due to the large variation in their topology and branch geometry. Prior models can provide means to perform statistics on coronaries by either looking into their characteristics on territories or by building statistical shape models to compute their modes of variation. Furthermore, statistical coronary shape models can be used in various applications such as coronary branch labeling and correlation between coronary artery diseases and coronary anatomy.

Traditional statistical methods are well suited for shapes sharing a common topology which is not the case for coronaries. More advanced methods are needed to build shape models that can consider both coronary topology and branch shape. The specific aims of this project are computing coronary distribution on territories and building tree-shape models and geodesic metrics that can account for topology and branch geometry.

1.2 Background

Coronary arteries travel along the surface of the heart and feed the heart muscles at different locations. Therefore, their spatial distribution over the heart surface can be correlated with their anatomical variations. Vessel density maps were computed in a previous work [2] to build spatial graphs for capturing branching patterns and anatomical spatial locations of intra-cranial vascular networks. Although vessel distributions on territories are valuable for probabilistic analysis, they do not account for the large variation in vessel *topology* which may be captured with statistical shape models.

Statistical shape models are used to represent the variations in the shape over a training set. They are built commonly by first aligning the shapes in the training set using a parametrized or landmark based shape model and then by modeling the statistical variations in this shape model using statistical methods such as well-known principal component analysis (PCA) for euclidean

manifolds, principal geodesic analysis (PGA) for non-euclidean manifolds and independent component analysis (ICA) which is a powerful latent variable model. However, these methods are well-suited for shapes sharing a common topology which is not the case for tree-like shapes. Although parameterization or landmark based definition of tree-shape structures are not possible, they can be represented as high-dimensional points in a geometric space to perform statistics on them.

One most important element of statistical shape analysis is the shape mean because it can best explain the entire training set and allows to compute the variability over it. However, there is not any ready definition of mean in tree-shapes because of their topological variability. In its classical definition, the mean of a set of points is the point which has the minimal sum of squared geodesic distance to other points in the set. Therefore, computing the tree-shape mean requires finding geodesic paths between points in the tree-shape space.

The best known method for computing geodesic deformation between tree-shapes is called tree edit distance (TED) [3]. TED defines the the geodesic distance as the minimum cost for deforming one tree to the second by simple tree operations such as adding, removing or deforming a branch. This metric was previously used for matching cerebral vessels [4], for comparing shapes via their shock graph representations [5] and for computing average medial axes of shapes via the simplest possible tree edit paths [6]. However, in TED metric, there are infinitely many geodesic paths between two tree-shapes and therefore TED based geodesic does not satisfy the local uniqueness property which is required when computing unique averages that are suitable for statistical analysis.

Wang et. al. [7] proposed another metric which is the weighted sum of two different metrics which compute topological distance using TED and branch geometry distance using Euclidean, respectively. They applied this metric to brain blood vessels by computing PCA which encodes the maximum variation in topology and branch geometry. However, since this metric does not simultaneously consider topology and branch geometry, it has discontinuities and topological changes have more cost than branch shape variations with constant topological structure. Therefore, this metric is not suitable for large trees with large topological variations and with noise such as spurious or missing branches.

Feragen et.al. proposed Quotient Euclidean Distance (QED) metric to compute *unique* geodesic deformations between tree-shapes by concatenating local tree deformations [8]. QED geodesic was then applied to airway average tree computation [9] and to airway tree matching [10]. In spite of its computational complexity, this geodesic metric has continuous and natural deformations and more importantly has a unique geodesic path which makes it suitable for statistical analysis.

1.3   Significance

The main contributions of this project are the presentation of results from coronary distribution over a common coordinate system and application of tree-shape geodesic deformations to coronary average tree computation and coronary tree matching. In addition, QED metric is extended to handle missing branches and is implemented computationally efficient allowing a large number
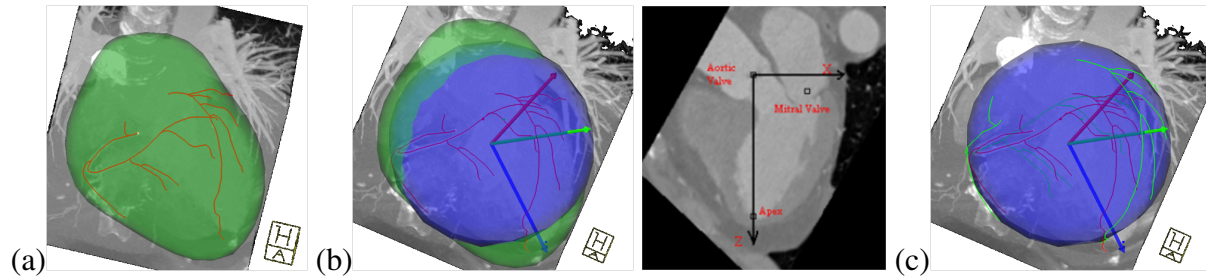
Figure 2: a) Sample input coronary centerlines and heart pericardium mesh. b) Fitted spherical model and canonical coordinate system axes. Main z axis is defined as the direction pointing from aortic valve center to the left ventricle apex. X axis is the vector perpendicular to z axis and lies on the plane formed by three landmarks. Y axis is the cross product of X and Z axes. c) Projected coronary centerlines (green) on the canonical surface.

of internal structural changes. The outcome of this project can yield future research for statistical analysis of coronary anatomy.

The outline of this report is as follows. First part of section 2 explains my work on coronary territories including the alignment of coronary centerlines and the coronary average density map computation. Following territories, TED and QED geodesic metrics are explained with implementation details. Section 2 ends with the application of these metrics to coronaries. Results are given following each subsection. Section 3 concludes this report.

2   Methods

2.1   Alignment of Coronary Centerlines

In this project, I received 50 hand annotated CTA coronary datasets with corresponding left and right coronary trees, heart pericardium mesh and anatomical landmarks from Siemens, Figure 2a. For statistical analysis, it is necessary to align the coronary centerlines in the training set. In my technical approach, this is achieved by first defining a canonical coordinate system by fitting spherical model to the heart pericardium mesh where the axes of this coordinate system are determined from three key anatomical landmark points, Figure 2b. Coronary centerlines are projected onto the canonical surface in order to find correspondence between them, Figure 2c. Finally, the projected coronary trees in the entire training set are aligned by first normalizing them to have unit radius and then transforming their centerlines based on the transformation computed from the rotation between their coordinate system axis to a reference axis chosen in the training set. Figure 3 shows left and right aligned coronary centerline trees.
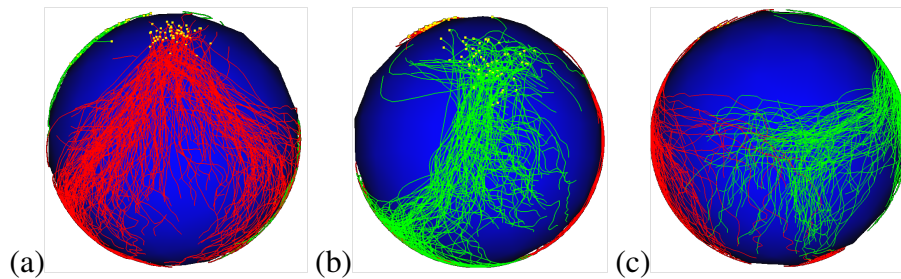
Figure 3: Aligned (a) left and (b) right coronary centerlines. Ostia points are depicted in yellow. (c) This figure shows the region where left or right coronaries feed posterior descending artery which also determines the dominancy of the circulation. The population has right dominant circulation which agrees with the general statistics stating 70% right dominancy.
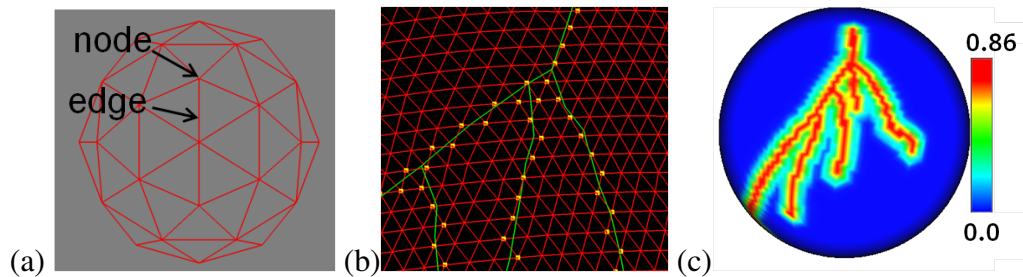

Figure 4: (a) Constructed graph on the recuresively triangulated mesh surface. (b) Coronary centerlines (green) are mapped to graph nodes (yellow). (c) Density map computed for a sample left coronary.

2.2 Statistics on Coronary Territories

2.2.1 Technical Approach

In this part of my project, I investigate the distribution of aligned coronary centerlines on the canonical surface by computing the average density map from the population. Density maps are computed from vessel distance maps which correspond to the great circle distance from discretized canonical surface points to the closest coronary centerline points. One way of discretizing the canonical surface is to parameterize it using discrete polar coordinates, however, this approach does not provide uniform sampling where the points are denser at the poles. In order to avoid this problem, my approach discretizes the canonical surface by recursively dividing it into smaller triangles starting from an octahedron, Figure 4a.

The triangulated mesh surface is then used to construct a graph $G = (N, E)$ with nodes N that correspond to vertices in the mesh and edges E that connect the neighboring vertices, Figure 4a. The graph edges are assigned with a cost computed from the great circle distance passing through their adjacent vertices. Since the underlying manifold is non-Euclidean, using great circle distance instead of Euclidean distance is important in order to have accurate results.

Coronary distance map is computed by running Dijkstra's algorithm on the constructed graph. Dijkstra's shortest path is a greedy algorithm which can compute globally minimal cost paths
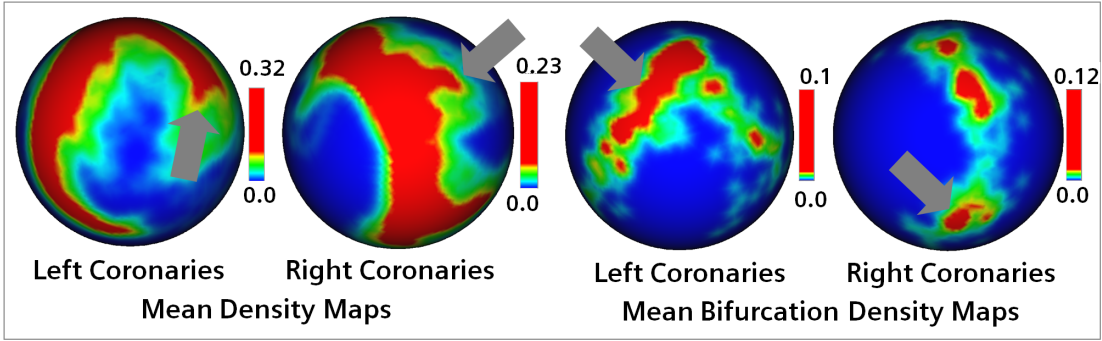
Figure 5: Coronary average density maps.

from a single source node to other nodes in an directed or undirected graph when the edge costs are non-negative. In my approach, coronary distance map, $D(\mathbf{x})$ is first initialized to infinity. Second, upsampled coronary centerline points are mapped on the graph by updating the distance of a node with its great circle distance to closest centerline point, Figure 4b. Dijkstra's algorithm is then run starting from this initial coronary distance map to obtain the final distance map. The intuition behind this approach is to consider the whole coronary centerline tree as a single source node in the graph and find the minimum cost path from this source node to all graph nodes. The density map $\rho(\mathbf{x})$ is computed from gaussian weighting of the distance map $D(\mathbf{x})$ with standard deviation σ, Eq.(1). Figure 4c shows computed density map for a sample coronary tree.

$$\rho(\mathbf{x}) = exp(-D(\mathbf{x})/\sigma^2) \qquad \overline{\rho}(\mathbf{x}) = \frac{1}{N}\sum_{i=1}^{N}\rho_i(\mathbf{x}) \qquad (1)$$

2.2.2 Experiments/Results

I computed density maps for both left and right coronary trees in 50 datasets and took their average $\overline{\rho}(\mathbf{x})$ in the population, Eq.(1). The σ parameter was chosen as 5mm which is large enough to have high densities in the coronary lumen. Figure 5a, b illustrate the average density maps. In order to observe the branching patterns on the territories, the average density map is recomputed by only mapping bifurcation points onto the graph. Figure 5c, d shows bifurcation average density map results.

These results show that the coronaries have a compact distribution over particular locations of the heart surface. Branching patterns are also visible in the average density maps. From Figure 5c, it is interesting to see that secondary coronaries branch off the proximal LAD uniformly.

2.3 Tree-shape Geodesic Paths via Tree Edit Distance Metric

2.3.1 Technical Approach

Tree edit distance is the best known metric to compute geodesic path between two trees. In this method, geodesic distance is computed as the minimal cost of deforming one tree to the second
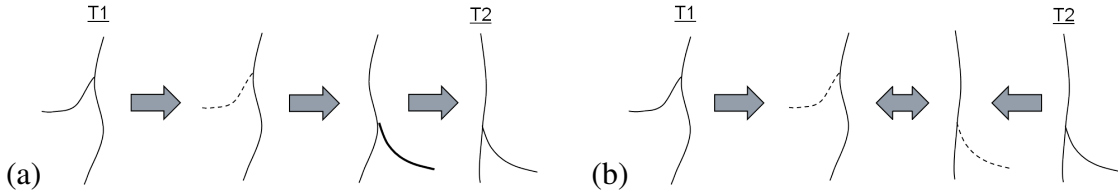
Figure 6: (a) Unidirectional and (b) Bidirectional TED based geodesic deformation.
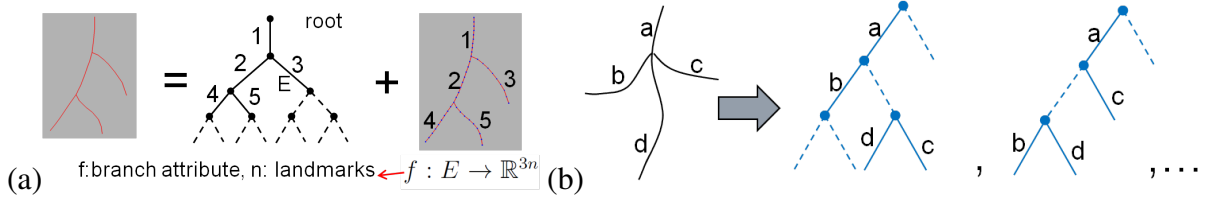

Figure 7: (a) Tree-shape representation (b) same non-binary tree-shape is represented with different binary trees.

one with basic edit operations such as adding, removing or deforming a branch. Figure 6a shows an example where the first tree is deformed to second one by first removing the secondary branch on the upper left side and then adding another secondary branch to bottom right, and finally deforming it to match the second tree. However, in such *unidirectional* deformation, there are infinitely many branches for adding operations which makes its implementation infeasible.

In *bidirectional* deformation, both trees are edited concurrently by only removing their branches until they are deformed to match eachother when they both correspond to the same topology, Figure 6b. This kind of deformation can achieve the same minimal cost as unidirectional deformation but the number of total editing operations remains constant as advantage. This idea was previously used in cerebral vessel matching [4]. Similarly, I use a bidirectional approach for TED based geodesic path computation.

In my technical approach, tree-shapes are represented similar to QED work in [8] where a tree-shape corresponds to a high-dimensional point in the Euclidean space and it is represented as a pair (T, f) of an ordered binary tree $T = (E, r)$ with edges E and a root point r, and branch attributes $f : E \rightarrow \mathbb{R}^{2n}$ where each edge E is mapped to n landmark points sampled along the matching branch geometry, Figure 7a. The Euclidean representation of the tree-shape space becomes $X = \prod_{e \in E} \mathbb{R}^{2n}$. The binary tree accounts for the tree-shape topology where non-binary tree-shapes can be represented via binary trees by collapsing their zero-attributed edges, Figure 7b.

In bidirectional TED method, one needs to determine whether two tree-shapes have the same topology or not. In my approach, a topology matching algorithm is designed which traverses the binary tree of the tree-shape using depth first search (DFS) and encodes 1 for each downstream visit and encodes 0 for each upstream visit. In order to take non-binary tree-shapes into account, the zero edges in the binary tree are bypassed and consecutive non-zero edges with no sibling edges are merged during DFS traversing, Figure 8.

The TED geodesic path is computed by running bi-directional Dijkstra's algorithm between
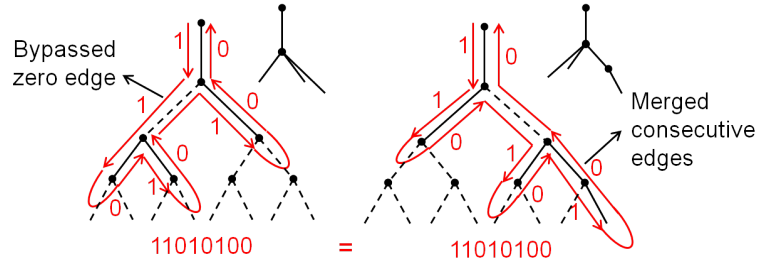
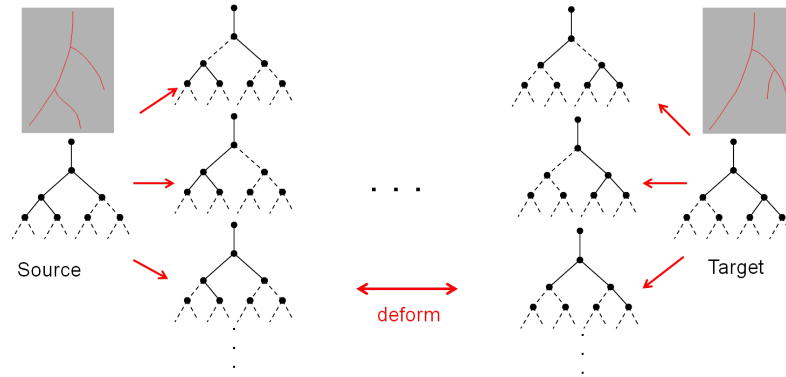Figure 8: (a) DFS encoding of the binary-tree for topology matching.

Figure 9: (a) Concurrent propagation of tree-shapes from source and target tree-shapes.

source and target tree-shapes. The common unidirectional Dijkstra propagates a minimum cost front from the source node until it hits the target node where bi-directional Dijkstra starts the propogations from both source and target nodes and grows them until their fronts collide with eachother. Similary, in this project, the propagations are started from source and target tree-shapes and their fronts are grown by removing branches from the tree-shapes. The propagations stop when two tree-shapes from different fronts with same topology collide with eachother. The tree-shapes are traced from the collision point back to the source and target nodes to obtain the geodesic path, Figure 9. In my implementation, the cost of deforming one branch to another is the Euclidean distance between their landmark vectors and removing a branch has the same cost as deforming it to a zero length branch.

For the application of TED to tree matching, branch labels from both tree-shapes are propagated through TED geodesic deformation by dropping the label on removed branches and finally matching the labels in the tree-shape deformation step.

2.4 Quotient Euclidean Distance Metric

2.4.1 Technical Approach

In the Euclidean tree-shape space mentioned in previous section, different points may correspond to the same tree-shape. In order to represent natural and continuous deformations between two
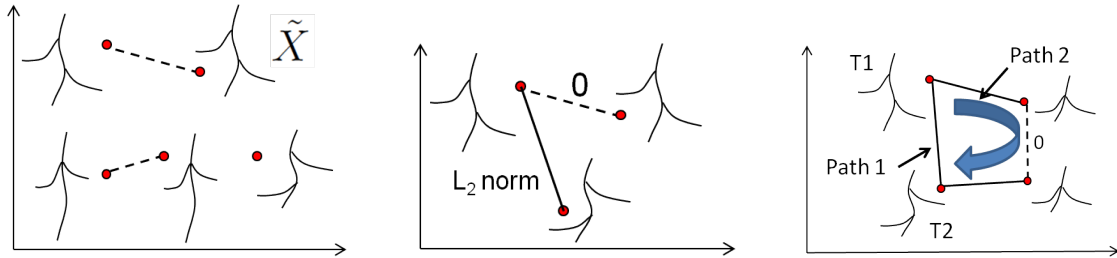
Figure 10: (a) Points corresponding to same tree-shape are identified in the Quotient Space (b) QED is zero when the tree-shape representations are identical otherwise it is L2 norm of branch costs. (c) Multiple paths exist between T1 and T2. First path directly connects both trees where the second path goes through internal structural transition. QED geodesic chooses the second path if the side branches are longer than the internal branch.
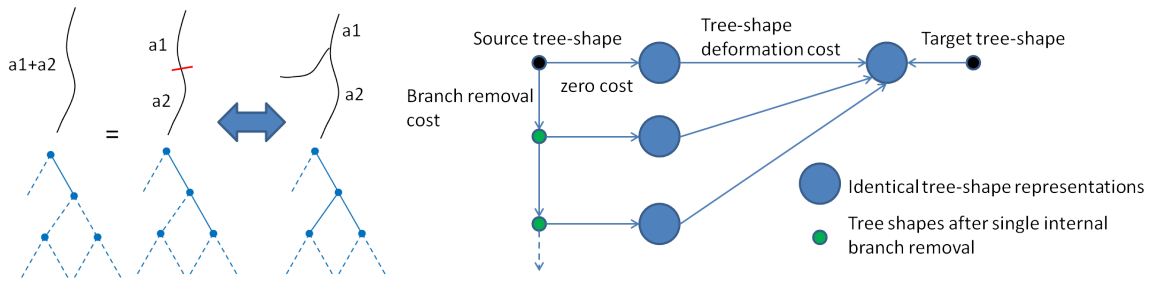

Figure 11: (a) Bottom wo binary tree representations of the left tree-shape are considered to be identical. Branch geometry is equally partitioned and mapped onto edge attributes. This allows matching left tree to the main branch of the right tree. (b) Constructed graph for QED geodesic computation.

tree-shapes with different topologies, the quotient space $\tilde{X}$ was defined in [8] where different representations of the same tree-shape are identified, Figure 10a. In this definition, two tree representations are identical if the attributed trees are exactly the same after collapsing zero-attributed edges, Figure 7b. In other words, the quotient space $\tilde{X}$ glues together all points in X that correspond to the same tree-shape.

The Euclidean distance in $\tilde{X}$ is called as Quotient Euclidean Distance (QED). In this metric, the distance between two different tree-shapes is computed from the Euclidean norm of the difference between their point vectors whereas the distance between identical trees is set to zero Figure 10b. It was also shown in [8] that the geodesic path between two points in this space follows the tree-shapes which only differ from eachother with internal topological changes, Figure 10c. This metric is well-behaved and proven to be unique in a previous work [8].

In my approach, the identical tree-shapes are defined slightly different than the definition above. Two tree-shape representations are considered to be identical if the attributed trees are exactly the same after collapsing zero-attributed edges and then *merging consecutive edges which do not have sibling edges*. This definition of quotient space allows handling missing branches, Figure 11a.

Dijkstra's algorithm is guaranteed to give globally minimum cost path between two nodes in a graph when the graph edges are non-negative. Therefore it is suitable for QED geodesic path computation since QED is a non-negative metric. In Dijsktra's algorithm, the distance map is initialized to infinity except the source node which has zero distance cost. The algorithm propagates its front by choosing the node with minimum distance cost (which is not previously chosen and marked) from a priority queue and updating the distance of its neighbors until the chosen node is the target node. In my QED geodesic implementation, the algorithm is initialized by adding identical representations of the source tree-shape to the priority queue with minimum QED distance to identical representations of the target tree-shape. In addition, tree-shapes obtained after removing single internal edge of source tree-shape are also added to the priority queue with branch removal cost. After initialization, the algorithm chooses the tree-shape with minimum distance cost in the priority queue which is then updated following similar steps as in the initialization. If the chosen tree-shape belongs to one of the identical representations of the target tree-shape, the algorithm returns its distance as the geodesic distance. The geodesic path is computed by back tracing from the target tree-shape. Figure 11b shows the constructed graph.

The uniqueness property of QED geodesic path makes this metric suitable for average tree computation. In the classical definition, the mean of a set of points in a Euclidean metric space (X, d) is the point which has the minimum squared distance sum to the points in the set.

$$\overline{\mathbf{x}} = \arg\min_{\mathbf{x}} \sum_{i=1}^{N} d(\mathbf{x}, \mathbf{x_i})^2 \tag{2}$$

There is no numerical solution to optimize the equation (2) for tree-shape space. However, the mean can be still approximated using iterative techniques such as weighted midpoint and

Source	Target tree/ Geodesic distance				Source	Target tree/ Geodesic distance				Source	Target tree/ Geodesic distance			
	6.9	10.8	13.9	15.1		6.8	8.9	13	13.3		3	3.5	4.6	5.5
	6.9	9.1	13	14.6		6.8	9	14.8	10.4		3	4.2	4.5	4.9
	6.4	10.8	13	14.6		8	8.9	10.4	14.7		2.8	3.5	4.2	4.9
	9.1	13.3	14.6	15.1		9	13.2	13.3	14.7		4.5	4.9	4.9	5.5
	6.4	13.3	13.8	14.6		8	13	13.2	14.8		2.8	4.6	4.9	4.9

a	b	c

Figure 12: Geodesic distances between sample 2D tree-shapes computed with (a) TED (Dijkstra approach) (b) QED with L1 norm cost and (c) QED with L2 norm cost.
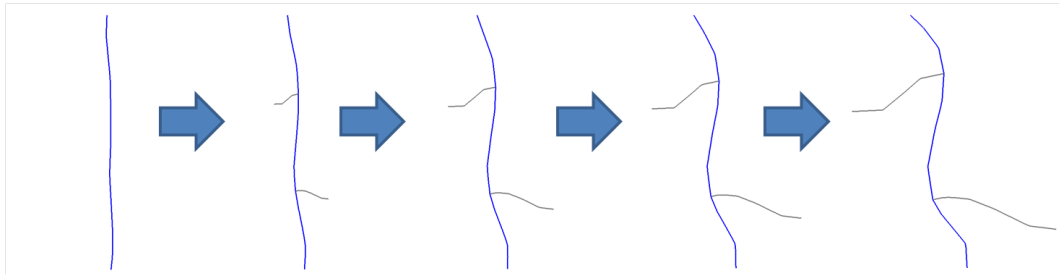

Figure 13: This figure shows the geodesic deformation between two tree-shapes where the two side branches are missing in the first tree.

birkhoff shortening. The first approach approximates the mean by iteratively computing the mean from weighted midpoints along the geodesics. The second approach, birkhoff shortening, recursively computes means of point pairs until there is only one point left. For this project, brikhoff shortening is used to compute the mean of tree-shapes, because our tree-shape representation has a limited depth and brikhoff shortening computes geodesic between tree-shapes with similar topological complexity where weighted midpoint always computes geodesics between the curent average tree and the next tree in the training set. Therefore, weighted midpoint approximation can be more prone to the order of trees.

For the application of QED to tree matching, branch labels from source tree are propagated along QED geodesic deformation by dropping the label on collapsed branches.

2.4.2 Experiments/Results

I implemented the TED geodesic metric using depth-5 binary trees. The method was run on ordered and rooted 2D tree-shapes where I implemented an algorithm to automatically detect the order of branches based on the angle of parent and children branches. 20 equidistant landmarks
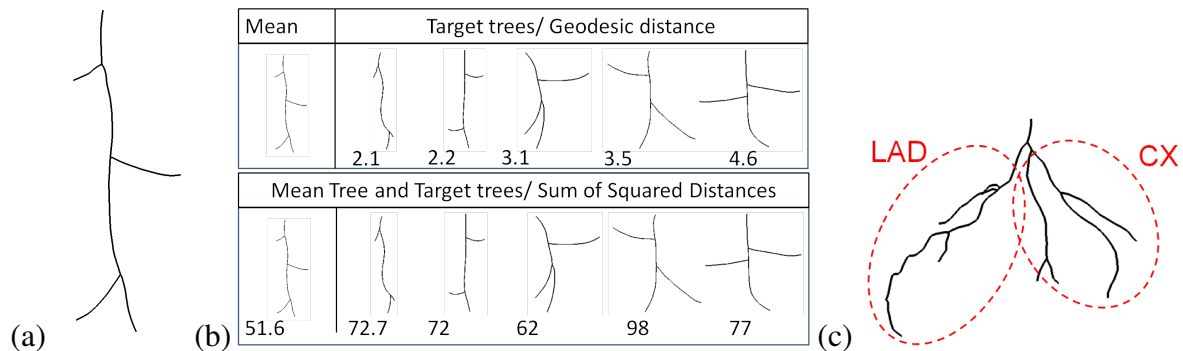
Figure 14: (a) QED average tree (b) distances from average tree to sample trees and sum of squared distances to entire set (bottom table). (c) Geodesic deformations are computed in LAD and CX subtrees separately.

points were sampled along each branch segment. The implemented method took less than 1sec to compute geodesic paths on my laptop with Intel i7 Core processor (1.86GHz) and 3GB RAM. Figure 12a shows TED geodesic distances between sample tree examples which I manually created and which were also used for presenting results in [8].

QED geodesics were computed using depth-4 binary trees and identical binary trees in quotient space were stored in local disk for computational efficiency, i.e., it took less than 5 sec on my laptop. Although my implementation supports depth-5 binary-trees, it takes around 10min to compute one geodesic path. These runtimes were recorded from my multi-threaded implementation where I used OpenMP to parallelize distance computations between all identical tree-shape pairs.

Figure 12b and c show QED geodesic distances with L1 norm and L2 norm cost function, respectively. These results are consistent wit the previously reported work in [8]. Feragen et. al. discusses that QED has same geodesic distance as TED when L1 norm cost is used. So, ideally, the computed distances from Dijkstra based TED and L1 Norm QED approaches should be the same. However, they are slightly different in the results table Figure 12a and b. This can be explained by different branch point sampling schemes used in my TED and QED implementations, i.e., in the TED implementation, branches are merged when possible and their landmark points are re-sampled whereas QED implementation keeps the original samplings. After all, the first matchings are same in both implementations. Please check movies on the course wiki web page for sample geodesic deformation movies.

Figure 13 illustrates an important example where two trees are matched correctly in spite of the two missing side branches in the first tree. This results shows the effectiveness of new definition of identical tree-shape space in my approach for handling missing branches.

Figure 14a shows the QED average tree computed from sample trees. The upper table in Figure 14b shows the distance from mean tree to sample trees. The sum of squared distances are listed in the bottom table. As expected from the classical definition of mean, average tree has the smallest sum of squared distances.

2.5 Application to Coronaries

In this part of my project, I apply TED and QED geodesic metrics to average coronary tree computation and coronary tree matching. As a first step, coronary centerlines in the training set are pruned because the implemented metrics support upto depth-5 trees. I implemented an algorithm to automatically prune a tree by iteratively removing shortest branches until its topology can be represented with a depth-3 binary tree. The reason of choosing depth-3 instead of supported binary trees with higher depths is that the intermediate trees along the geodesic path may have more depth than the end-point trees. Pruning is applied to right tree itself, and to left anterior descending (LAD) and circumflex (CX) subtrees of the left tree separately. Each branch is sampled with 20 landmark points.

TED and QED metrics are customized for 2D spherical manifolds by replacing the Euclidean distance with Great Circle distance. Coronary branch orders are detected automatically similar to my approach described for 2D trees that lie on planar surface. Since the coronary main, LAD main and CX main branches are seen in every coronaries in the population, these branches are fixed and the geodesic deformations are computed only within the subtrees, Figure 14c.

2.5.1 Average Coronary Tree Computation

Average left and right coronary trees were computed from 40 coronary examples out of available 50 examples where 10 of them were discarded due to the large variation in the segmentation, i.e., left coronary centerlines which have a single short LAD or CX branch were discarded. Figure 15a shows left and right average coronary trees. The average trees consist of most commonly seen branches in the population. For comparison purposes, average trees were recomputed using TED (QED with L1 norm cost), Figure 15b. According to [8], TED metric is more prone to internal topological changes. This is consistent with my results where the TED average tree has less number of branches as it prefers flipping side branches rather than growing them.

In order to assign membership scores to an unseen coronary tree, my initially proposed approach was to compare its distance to average tree with the mean distance from the population to average tree. However, the underlying geometric space is high-dimensional which increases the likelihood of points being equidistant. In addition, the distance to average tree varies with the size of the coronary tree, i.e., a left coronary which has longer LAD or CX branch may have larger distance to average tree. Therefore, the geodesic distance to average tree is not sufficient for assigning membership scores itself.

2.5.2 Coronary Tree Matching

I applied both TED and QED geodesic deformation for coronary tree matching where labels from source tree are matched to target tree. Figure 16 shows labeling results by matching sample trees to average trees. QED deformation gives better labeling results than TED in these examples.
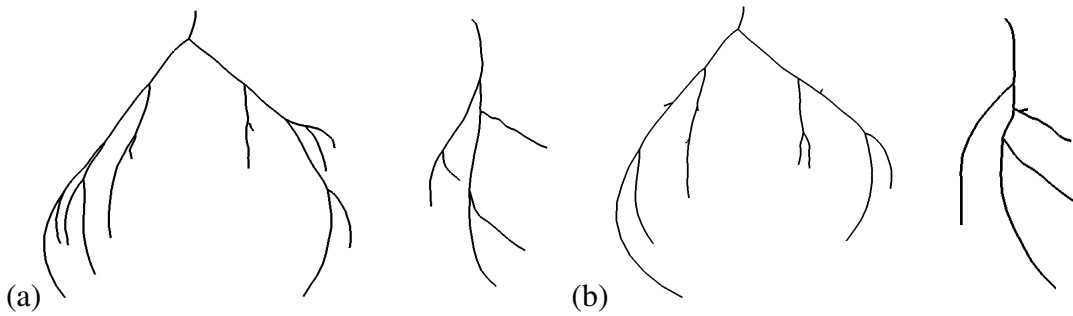
Figure 15: (a) Left and right coronary average tree (b) average trees are recomputed with TED metric.

3 Conclusion

In this project, I developed and implemented methods for investigating prior models on coronary arteries by looking at their distribution on territories and by building geodesic tree-shape metrics for coronary average tree computation and coronary tree matching. The results are evaluated in hand drawn ground truth trees and in a coronary training set. The methods are validated both visually and by comparing to related previous works. QED metric is extended to handle missing branches which improved the accuracy of results, especially, in tree matching.

As a future work, the coronary tree matching method can be evaluated using expert labeled coronary trees. This will also allow an adequate comparison of TED and QED based labeling accuracies. In addition, the QED computations can be done in depth-5 trees and be compared to current results.

Another future work would be to correlate coronary average tree with coronary anatomy for evaluating its topology, i.e., to see how realistic its branches are. Furthermore, gathering statistics such as coronary attributes, pathologies from spefcic patient data and mapping them onto the average tree would be another interesting future work. This work can highlight certain anatomical locations with high risk of pathologies such as stenosis.

Finally, the integration of developed prior coronary models, including density maps and tree-shape models, into local tracking or global detection algorithms can be investigated in a future work.

4 Management Summary

4.1 Deliverables

I achieved all minimum, expected and maximum deliverables of my project. I implemented my technical approaches into a research prototype that I developed using Siemens' Extensible Imaging Platform (XIP). All the results presented in this report were produced by using this research prototype.

My first minimum delivarable was the alignment of coronary centerlines into a common co-
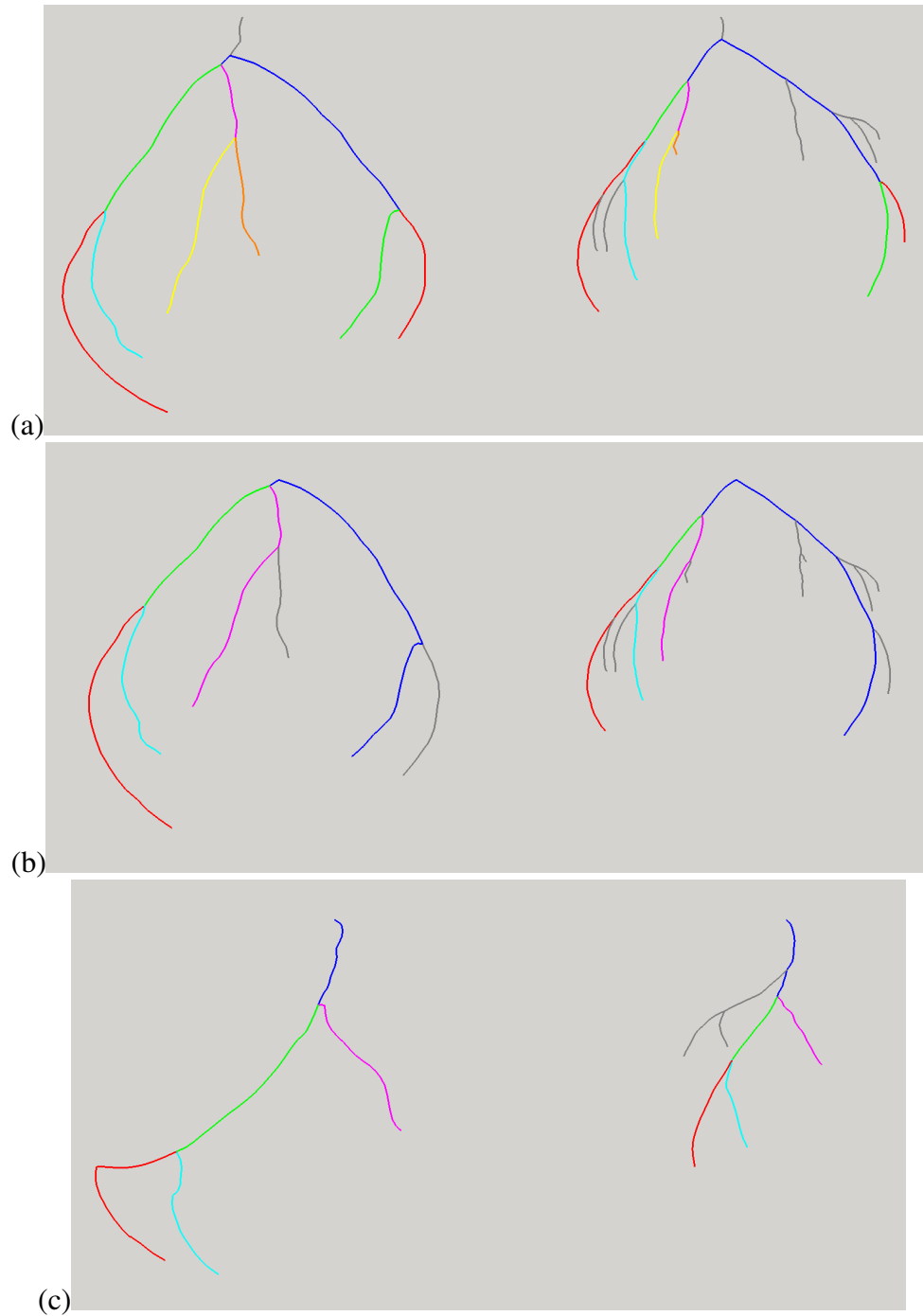
Figure 16: Matched branches are shown in same color and gray branches do not have correspondence. LAD and CX subtrees are matched separately. Matching a sample tree to left average tree (a) with QED (b) with TED. (c) matching to right average tree.

ordinate system. A set of coronary centerlines can be loaded into the prototype with single click which are then automatically aligned based on the method described in my technical approach. The prototype provides means to validate the alignment using 3D display of canonical coordinate system and the projected centerlines. My second minimum delivarable was the computation of coronary average density map. The prototype computes density maps automatically right after alignment step and displays color coded overlay of results for validation.

My expected deliverables were the computation of TED and QED geodesic metrics for depth-3 trees. The prototype can compute the geodesic deformation between two depth-3 trees using TED and QED metrics, and displays the geodesic distance and its path. It can also compute the average tree from a list of trees. The branch segments are color coded in order to observe matched branches. I implemented a tool to draw 2D trees for getting results. I validated my implementation by creatin sample trees that were used in another paper in which QED method was initially proposed.

I applied TED and QED metrics to coronaries for my maximum deliverables. The prototype can compute the average coronary tree from a list of coronary centerlines and match any two coronary trees after computing geodesic deformation between them. I experimented membership score assignment to an unseen coronary tree based on its distance to average tree. This allowed me to understand the nature of the problem. In addition to my maximum deliverables, I applied QED metric to coronary tree matching and compared the results to TED tree matching.

4.2   Lessons Learned

Through this project, I have learned that vascular structures may have very complex topology with large variation. Therefore, well known statistical shape analysis methods cannot be easily applied to them. In addition, I learned a new way of building statistical shape models and consolidated my knowledge of traditional landmark based methods. This project also showed me that a good design and implementation can make a very big difference in the computational efficiency which is important, especially, while working on a short-term result-oriented project.

References

[1] Donald Lloyd-Jones, Robert J Adams, Todd M Brown, Mercedes Carnethon, Shifan Dai, Giovanni De Simone, T Bruce Ferguson, Earl Ford, Karen Furie, Cathleen Gillespie, and et al. Executive summary: heart disease and stroke statistics–2010 update: a report from the american heart association. *Circulation*, 121(7):188–197, 2010.

[2] Stephen R. Aylward, Julien Jomier, Christelle Vivert, Vincent LeDigarcher, and Elizabeth Bullitt. Spatial graphs for intra-cranial vascular network characterization, generation, and discrimination. In *MICCAI*, pages 59–66, 2005.

[3] Philip Bille. A survey on tree edit distance and related problems. *Theor. Comput. Sci.*, 337:217–239, June 2005.

[4] W H Tang and Albert C S Chung. Cerebral vascular tree matching of 3d-ra data based on tree edit distance. *Medical Imaging and Augmented Reality*, page 116123, 2006.

[5] Thomas Sebastian, Philip Klein, and Benjamin B. Kimia. Recognition of shapes by editing their shock graphs. *PAMI*, 26:551–571, May 2004.

[6] Nhon H. Trinh and Benjamin B. Kimia. Learning prototypical shapes for object categories. In *Proceedings of CVPR Workshop on Structured Models in Computer Vision (SMiCV'10)*. IEEE, IEEE, June 2010.

[7] Haonan Wang and J S Marron. Object oriented data analysis: Sets of trees. *Annals of Statistics*, 35(5):1849–1873, 2007.

[8] Aasa Feragen, Francois Lauze, Pechin Lo, Marleen de Bruijne, and Mads Nielsen. Geometries on spaces of treelike shapes. In *Proceedings of the 10th Asian conference on Computer vision - Volume Part II*, ACCV'10, pages 160–173, Berlin, Heidelberg, 2011. Springer-Verlag.

[9] Aasa Feragen, Søren Hauberg, Mads Nielsen, and François Lauze. Means in spaces of tree-like shapes. In *ICCV*, pages 736–746, 2011.

[10] A. Feragen, P. Lo, V. Gorbunova, M. Nielsen, A. Dirksen, F. Lauze, and M. de Bruijne. An airway tree-shape model for geodesic airway branch labeling. In *Third MICCAI Workshop on Mathematical Foundations of Computational Anatomy*, 2011.